THE JOURNAL OF BIOLOGICAL CHEMISTRY
Vol. 279, No. 6, Issue of February 6, pp. 4358–4365, 2004

Printed in U.S.A.

Dynamic Regulation of the Inducible Nitric-oxide Synthase by NO

COMPARISON WITH THE ENDOTHELIAL ISOFORM*

Received for publication, May 14, 2003, and in revised form, October 30, 2003
Published, JBC Papers in Press, October 31, 2003, DOI 10.1074/jbc.M305048200

Clement Gautier‡, Michel Négrerie‡, Zhi-Qiang Wang§, Jean-Christophe Lambry‡, Dennis J. Stuehr§, Fabrice Collin‡, Jean-Louis Martin‡, and Anny Slama-Schwok‡¶

From the ‡Laboratory for Optics and Biosciences, INSERM U451, CNRS Unite Mixte de Recherche 7645, Ecole Polytechnique, 91128 Palaiseau Cedex, France and §Department of Immunology, Lerner Research Institute, Cleveland Clinic Foundation, Cleveland, Ohio 44195

We studied by ultrafast time-resolved absorption spectroscopy the geminate recombination of NO to the oxygenase domain of the inducible NO synthase, iNOSoxy, and to mutated proteins at position Trp-457. This tryptophan interacts with the tetrahydrobiopterin cofactor BH_4, and W457A/F mutations largely reduced the catalytic formation of NO. BH_4 decreases the rate of NO rebinding to the ferric iNOSoxy compared with that measured in its absence. The pterin has a larger effect on W457A/F than on the WT protein by increasing NO release from the protein. Therefore, BH_4 raises the energy barrier for NO recombination to the mutated proteins in contrast with our observations on eNOS (Slama-Schwok, A., Négrerie, M., Berka, V., Lambry, J.-C., Tsai, A.-L., Vos, M., and Martin, J.-L. (2002) *J. Biol. Chem.* 277, 7581–7586). Thus, we show a differential effect of BH_4 on NO release from eNOS and iNOS. Compared with the position of this residue in the BH_4-repleted enzyme, simulations of the NO dissociation dynamics point out at a swing of Trp-457 toward the missing pterin in the absence of BH_4. NO geminate-rebinding data show a more efficient NO release from eNOS than from iNOS once NO is formed. Consistently, NO produced by iNOS is regulated by its ferric nitrosyl complex in contrast with eNOS. We show that the small enhancement of the NO geminate recombination rate in W457A/F compared with that in the WT enzyme cannot explain the decrease of NO yield because of the mutation; the major effect of the mutation thus arises from an uncoupled catalysis (Wang, Z. Q., Wei, C. C., Ghosh, S., Meade, A. L., Hemann, C., Hille, R., and Stuehr, D. J. (2001) *Biochemistry* 40, 12819–12825).

The inducible NO-synthase (iNOS),[1] best characterized from macrophages, generates the highest NO concentration among the three isoforms of NOS. High NO concentrations counter pathogens by their cytotoxicity and taking part in the response of the immune system. In contrast, the constitutive isoforms, the neuronal nNOS and, especially, the endothelial eNOS produce NO at low concentrations, which acts as a physiological signal in vasorelaxation, neurotransmission, and oxygen detection (1).

The NOS enzymes utilize NADPH as a donor of electrons, arginine, and oxygen as co-substrates (2). The cofactor tetrahydrobiopterin BH_4 is required for NO production and strongly decreases the level of superoxide ions formed by NOS in its absence (3). The binding of BH_4 to iNOS has structural effects in promoting the enzyme dimerization (4–6), in increasing the binding affinity for the substrate, in shifting the heme spin state from low spin to high spin (7), and in modifying the heme midpoint potential (8). In addition to these structural roles, BH_4 is involved in the catalysis as an electron donor to Fe(II)-O_2 complex (9–11). Direct evidence for a pterin radical was obtained by rapid freeze-quench EPR (12).

According to the x-ray structures of iNOS oxygenase domain, BH_4 makes hydrogen bonds with the heme propionate and extensive interactions with the residues Trp-455, Trp-457, Phe-470, Arg-375, and Arg-193 (13–16). Mutation of the residues located near the BH_4 binding site in the oxygenase domain of iNOS shows that hydrogen bonding and stacking modify the extent of dimer formation, the heme environment, and the efficiency of NO synthesis. Specifically, the mutation of Trp-457 into Phe and Ala allowed for dimerization but decreased the NO synthesis activity 3.3-fold and 8-fold, respectively (17). Single-turnover experiments using these mutated proteins followed the formation and decay of Fe(II)-O_2 and the BH_4 radical as intermediates, yielding the ferric complex as the final species (18–19). These studies showed that Trp-457 ensured a correct rate of electron transfer from BH_4 to Fe(II)-O_2 in the presence of arginine, which maximized the extent of *N*-hydroxyarginine formed. In the second step of catalysis, Trp-457 modulated the kinetics of *N*-hydroxyarginine oxidation by iNOS, although the BH_4 radical was not detectable (in the millisecond time scale). However, the rate of Fe(II)-O_2 decay was coupled with the rate of citrulline formation. The amount of citrulline per heme decreased to 54 and 38% in W457F and W457A, respectively, compared with the wild type.

Several publications characterized a reversible inhibition of iNOS related to the heme binding of self-generated NO. During steady-state catalysis, the ferric nitrosyl complex mainly accumulated, whereas during the first seconds of catalysis, the ferrous-NO complex has also been detected (12, 20). Heme-NO complex buildup was biphasic, with a fast "pre-equilibrium" phase of all newly formed NO binding to the ferric NOS heme before leaving the active site. This phase accounted for about 30% of the absorption changes, whereas a slower phase occurring in the tens of seconds reflected the binding of NO that builds up in solution to the ferric heme. Modeling studies of NOS catalysis could reproduce these phases (21).

In this report, we study the geminate recombination of NO to the ferric and ferrous states of iNOSoxy (WT). NO recombines much faster to the ferrous heme than to the ferric heme of

* The costs of publication of this article were defrayed in part by the payment of page charges. This article must therefore be hereby marked "*advertisement*" in accordance with 18 U.S.C. Section 1734 solely to indicate this fact.

¶ To whom correspondence should be addressed. Tel.: 331-6933-3101; Fax: 331-6933-3017; E-mail: anny.schwok@polytechnique.fr.

[1] The abbreviations used are: iNOS, inducible NO-synthase; iNOSoxy, oxygenase domain of iNOS; WT, wild type; eNOS, endothelial NO-synthase; BH_4, (6R)5,6,7,8-tetrahydrobiopterin; DTT, 1,4 dithiothreitol.

iNOS, in contrast with eNOS. This fact is consistent with the specificity of the catalysis of both isoforms. We also found differential effects of the tetrahydrobiopterin cofactor on NO release from iNOS and eNOS. These results are discussed from the perspective of simulations of the molecular dynamics.

We also studied the mutated proteins W457F and W457A to check whether the large decrease in NO yield induced by the Trp mutation can be partly accounted for by modifications of NO release. Our results clearly show that the mutation has a minimal effect on the rate and extent of NO release and mainly reduces the efficiency of the catalysis.

EXPERIMENTAL PROCEDURES

Materials—L-arginine, (6R)5,6,7,8-tetrahydrobiopterin (BH_4), as well as chemicals used for the HEPES buffer, DTT, sodium dithionite, potassium ferricyanide, and glycerol were purchased from Sigma. NO gas diluted at 1% or 10% in argon, pure NO (99.999%) and high purity argon (99.9995%) were obtained from Air Product or Alpha Gaz.

Expression of the Enzymes—Wild-type and mutant iNOSoxy Δ-65 proteins (amino acids 66–498 plus a six His tag extension at the C terminus) were over-expressed in BL21 cells using the pCWori vector and purified as reported previously (17).

Preparation of Samples for Spectroscopy—A concentrated solution of wild-type iNOSoxy or Trp-457 mutants (at a final concentration of 67 μM) in 50 mM HEPES buffer, pH 7.5, and 5% glycerol was mixed with 1 or 20 mM arginine in an optical cuvette with a 1-mm path length. It was sealed with a rubber stopper and degassed by repetitive cycles of vacuum and argon. Anaerobic solutions of 1 mM BH_4 and DTT (3 mM final concentration) were added to the protein containing arginine when BH_4-repleted samples were needed. The concentration of BH_4 was determined by its absorbance at 298 nm ($\epsilon_{298} = 9.4 \times 10^3$ M^{-1} cm^{-1}) measured in the HEPES buffer at pH = 7.5 and found to be similar to the reported value (22). The solution was then incubated overnight on ice to allow completeness of the equilibration. NO gas was then introduced in the cell at a pressure of 1.3 bar using a gas train. When experiments with the reduced enzyme were performed, a slight molar excess of dithionite solution (that was previously titrated with potassium ferricyanide) was used. Depending on the NO concentration used, it was sometimes necessary to add more dithionite (2 to 3 equivalents) to achieve a stable ferrous-nitrosyl complex during the course of our laser experiment.

Time-resolved Spectroscopy—Time-resolved spectroscopy was performed with a 30 Hz pump-probe laser set-up described previously (23). Photodissociation of NO-bound iNOS was achieved by an excitation pulse at 582 nm, with a pulse width of 40 fs. The transient spectrum detected after a variable delay was probed with a white light continuum pulse, whose group velocity dispersion was minimized at 400 nm by a set of prisms. The wavelength calibration of the charge-coupled device camera was checked every day by using a thin-band filter. 25 scans were simultaneously recorded in three time windows: 50 ps, 500 ps, and 2 or 4 ns. Carbon monoxide bound to reduced myoglobin was monitored under the same conditions and used as a reference of flat kinetics in the time scales of 500 ps to 4 ns (24). Analysis of the data was performed by singular matrix decomposition of the time-wavelength matrix (25).

Molecular Dynamics Simulations—The modeling was performed by using the CHARMM27 software on an HP J5600 computer. The calculations used the file for Protein Data Bank ID code 1NSI (26–28). The dimer was composed of two identical chains of 431 residues each, two iron protoporphyrins, one Zn atom at the dimer interface, two NO ligands, two BH_4 and arginine molecules, 279 water molecules from the x-ray data, to which a "bath" of 4035 water molecules was added. Hydrogen atoms were generated by using the CHARMM HBUILD command. The energy of the structure was minimized. A relative dielectric constant equal to unity was applied to the entire structure. The equations of motion were numerically integrated using the Verlet algorithm with 1-fs time steps. To prepare simulations, an initial heating from 0 to 300°K was performed, and the speed of the atoms was calculated according to a Maxwell distribution. An equilibration at 300°K was then achieved in five steps of 50 ps each, allowing us to obtain a stable starting structure to perform the simulations of the NO dissociation. To simulate NO dissociation, the sudden approximation was used, by deleting the Fe-NO bond. The structure was allowed to relax during 10 to 20 ps, by incremental steps of 1 fs. Four trajectories of 10 ps, representing eight dissociation events, were performed for BH_4-bound iNOSoxy. Two trajectories of 10 and 20 ps were calculated for iNOSoxy without cofactor.

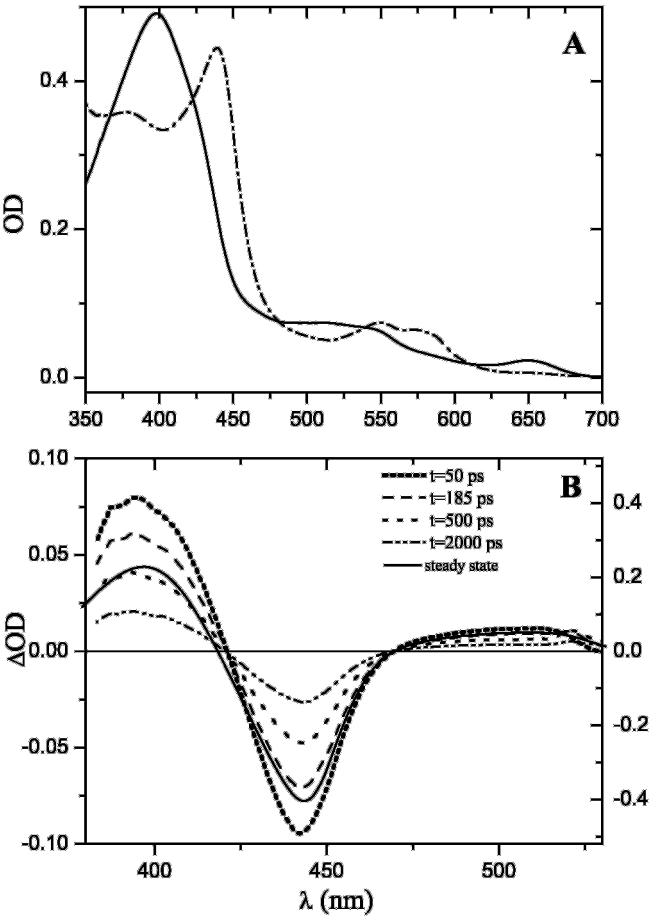

FIG. 1. *A*, absorption spectra of iNOSoxy in its ferric form and its nitrosyl complex. *Solid line*, argon-saturated solution of iNOSoxy in the presence of 1 mM BH_4; *dashed and dotted line*: same solution at 10% NO in the gas phase, 67 μM iNOSoxy, 50 mM HEPES, pH 7.5, 5% glycerol, and 20 mM arginine. *B*, transient absorption spectra obtained at various times after photodissociation of NO from iNOSoxy. *Left scale*, transient spectra monitored at t = 50 ps, *bold dotted line*; t = 185 ps, *dashed line*; t = 500 ps, *dotted line*; and *dashed and dotted line*, t = 2 ns. Superimposed and represented on the *right scale* is the steady-state absorption difference between the unliganded and the NO-bound ferric heme, shown as a *thin solid line*. 67 μM iNOSoxy, 50 mM HEPES, pH 7.5, 5% glycerol, in the presence of 20 mM arginine, 1 mM BH_4, 3 mM DTT, and 10% NO in the gas phase.

RESULTS

Effect of the BH_4 Concentration on the WT Ferric iNOSoxy

Steady-state Absorption—The wild-type iNOSoxy protein presents a maximum of the Soret band at λ_{max} = 422 nm without substrate and the BH_4 cofactor. This peak accounts for the low spin state of the sample. The addition of 20 mM arginine alone induces a partial shift from 422 nm to a broad maximum of the Soret band around 402 nm and a marked shoulder at 422 nm (29). Addition of 1 mM of BH_4 in the presence of DTT completely shifts the protein to high spin: the Soret band then peaks at 395 nm (5).

NO binding shifts the Soret maximum to 440 nm, and two Q bands are observed at 548 and 575 nm (Fig. 1). The NO complexes of the protein in the presence of arginine alone or with both arginine and BH_4 are stable.

Transient Absorption—Our laser set-up allowed us to cleave selectively the iron-NO bond by excitation of the complex at 582 nm, a wavelength located within one of the Q bands of the nitrosyl complex (λ_{max} = 575 nm). This bond cleavage is effective within the pulse width (40 fs). We then followed the ab-

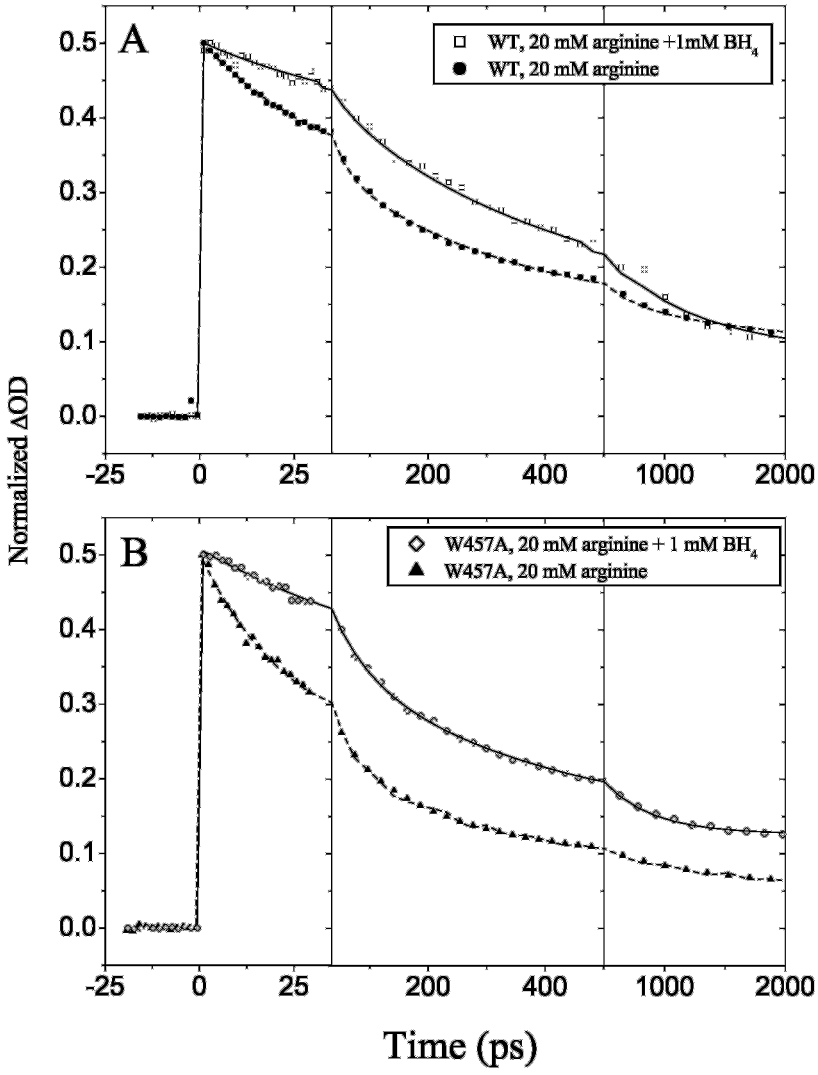

FIG. 2. **Effect of the presence or absence of 1 mM BH_4 on the kinetics of geminate recombination of NO to the ferric iNOSoxy and W457A.** *A*, WT in the presence of 20 mM arginine: □, with BH_4; ●, without BH_4. *B*, W457A in the presence of 20 mM arginine: ◇, with BH_4; ▲, without BH_4. 67 μM iNOSoxy or W457A, 1 mM BH_4, 3 mM DTT, 50 mM HEPES, pH 7.5, 5% glycerol. The data represent the first and predominant singular value matrix decomposition component. The fit of the experimental data by three exponential components is shown by a *solid line* (+BH_4) or a *dashed line* (−BH_4), as described in Table I.

sorption changes associated with NO rebinding to the heme. These changes corresponded to an absorption difference at a given time relative to that before the laser shot. In our experiment, we measured the geminate recombination that involves the rebinding of photo-dissociated NO molecules prior to their escape from the protein into the solvent. This takes place in the time scale of a few ps to 4 ns. We did not follow the slower phase, occurring in milliseconds, because of NO recombination with the heme after its escape into the solvent, which is a bimolecular reaction.

The transient spectrum presented a maximum absorption at 397 nm, a bleaching with a minimum at 442 nm, and two isosbestic points at 421 and 469 nm (Fig. 1). This result held true with or without 1 mM BH_4. These spectral features are characteristic of the ferric unliganded iNOSoxy with some quantitative differences. The steady-state difference spectrum presents the same extrema, but the intensity of the peak at 397 nm is somewhat smaller than the transient one, and the isosbestic point is blue-shifted to 418 nm. The latter differences are more marked in the absence of BH_4 (data not shown). Thus, in the steady state, there is a mixed population between low- and high-spin species, depending on the BH_4 content in the absence of NO. Once NO is bound, the ferric species turn to purely high spin, evidenced in the transient spectra. They retain their shape, and their amplitude decreases with time. Thus, the kinetics is associated with the decay of the same ferric species in a high-spin state that undergoes geminate recombination.

The geminate recombination of NO to the ferric heme of iNOSoxy involves two phases: a fast phase occurring in picoseconds, and a slower step taking place in nanoseconds (Fig. 2). This multi-exponential decay does not come from the heterogeneity in the dimer population. Indeed, the concentration of 70 μM of protein used in our experiments insured that iNOSoxy and W457A/F were dimeric. Indeed, 0.1 μM protein already formed 60, 70, and >90% dimer, respectively, for W457F, W457A, and iNOSoxy in the presence of 20 mM arginine (17).

The fast phase is best fitted by two exponentials, $\tau_1 = 50 \pm 5$ ps, and $\tau_2 = 425 \pm 25$ ps; the long component is $\tau_3 = 1.7 \pm 0.2$ ns, obtained with arginine and the cofactor. The A_4 asymptotic value represents the upper limit of the probability of NO escape from the protein without rebinding. Thus, about 13% of the photodissociated NO molecules are able to escape geminate recombination in the presence of arginine.

The rate of NO rebinding to the heme depended upon the BH_4 concentration (Fig. 2). The extent of decay decreased in the tens of picoseconds but increased in the hundreds of picoseconds in the absence of BH_4, compared with that at 1 mM BH_4. In addition, the lifetimes τ_1 and τ_2 are larger with the cofactor than without (Fig. 2*A* and Table I). Similar results were obtained by changing the arginine concentration from 20 mM to 1 mM, while BH_4 was kept constant at 1 mM (data not shown). Nonetheless, the kinetics reached a similar extent of decay after about 2 ns, *i.e.* 80% decay independently of the BH_4 concentration used. The kinetics were independent of the NO

TABLE I

Kinetic parameters were obtained by fitting the main singular value decomposition component with three exponents and a constant

The kinetic experiments were performed using 67 μM of the oxygenase domain of the enzymes iNOSoxy wild type (WT) or W457F/A mutants, 50 mM HEPES pH 7.5, and 5% glycerol.

Sample	Arginine	BH_4	τ_1	A_1[a]	τ_2	A_2[a]	τ_3	A_3[a]	A_4[a]
	mM	*mM*	*ps*		*ps*		*ps*		
WT[b]	20	0	30	0.32	286	0.38	3200	0.20	0.12
WT[c]	20	0	34	0.32	325	0.36	3180	0.19	0.13
WT[b]	20	1	50	0.15	425	0.48	1710	0.24	0.13
W457A[b]	20	0	20	0.39	138	0.34	1107	0.17	0.10
W457A[b]	20	1	44	0.18	210	0.36	740	0.21	0.25
W457F[b]	20	0	24	0.37	202	0.36	2000	0.15	0.12
W457F[c]	20	0	33	0.27	193	0.38	1704	0.17	0.18
W457F[b]	20	1	55	0.26	265	0.34	2093	0.17	0.23
WT red[c]	20	10	42	0.34	214	0.37	1722	0.27	0.02
WT red[b]	20	10	38	0.34	205	0.34	1590	0.32	0
W457A red[b]	20	1	28	0.55	338	0.41			0.04
W457A red[b]	20	10	34	0.52	356	0.42			0.06
W457F red[d]	20	1	32	0.54	314	0.43			0.03
W457F red[c]	20	1	40	0.58	483	0.42			0.09
W457F red[b]	20	1	35	0.54	283	0.40			0.06

[a] Relative amplitude, $A_1 + A_2 + A_3 + A_4 = 1$, not including the amplitude of the transient due to the excited state.
[b] NO 10% in the gas phase.
[c] NO 1% in the gas phase.
[d] NO 0.1% in the gas phase.

concentration in the range 1–10% in the gas phase (Table I and data not shown).

Effect of the BH_4 Concentration on the Mutated Proteins W457A/F

The affinity for both arginine and BH_4 was lower for the mutated proteins W457A/F than for the wild type (17). We measured the absorbance of the Soret band of W457A at different concentrations of BH_4 in the presence of 20 mM arginine. The shift from 423 to 395 nm was nearly reached at 1 mM BH_4; it was achieved at 3 mM BH_4 (data not shown).

The geminate recombination was clearly much faster without than with 1 mM BH_4, following a similar qualitative trend as that seen for the wild-type protein (Fig. 2, *A* and *B* and Table I). A large effect of BH_4 is observed in the first exponential, both in its lifetime varying from $\tau_1 = 20$ to 44 ps and in its amplitude $A_1 = 0.39$ to 0.18 in the absence/presence of BH_4 respectively. The addition of 1 mM BH_4 also increased the constant term compared with that obtained in BH_4-free solutions (Fig. 2*B* and Table I). This contrasts with the lack of such an effect in the wild-type enzyme. The mutated protein W457F followed a similar behavior than W457A with respect to the effect of BH_4 on the geminate recombination rate (Table I).

Effect of the Heme Redox State on the Geminate Recombination

The transient absorption of the reduced iNOS is red-shifted to 407 nm compared with that of the oxidized protein peaking at 397 nm. This maximum at 407 nm is close to that observed in the steady-state absorption $\lambda_{max} = 410$ nm. The geminate recombination of NO to the reduced heme, shown in Fig. 3, is best fitted by three exponential terms, $\tau_1 = 40 \pm 2$ ps, $\tau_2 = 210 \pm 10$ ps, and $\tau_3 = 1650 \pm 80$ ps. The same parameters were obtained within experimental error at either 1 or 10 mM BH_4 in the presence of dithionite (data not shown). The constant term is close to zero, thus none of the dissociated NO molecules escaped geminate recombination when the heme was in its ferrous state.

Fig. 3*A* compares the geminate rebinding of NO to iNOS as a function of its redox state. The rate of NO rebinding to the ferrous heme is faster relative to that of the corresponding ferric species. The pre-exponential term A_1 increases from 0.15 to 0.34, and the second lifetime τ_2 decreases from 425 to 210 ps in the ferric compared with the ferrous state. Moreover, the NO rebinding is complete when the heme is reduced, in contrast with a probability reaching 13% of NO escape from rebinding for the oxidized species. Fig. 3*B* shows that the extent of NO recombination is much lower in eNOS enzyme than in iNOS. The effect of the redox state on the geminate rebinding of both NOS isoforms will be discussed below.

Effect of the Trp-457 Mutation on NO Rebinding to the Ferric and Ferrous iNOSoxy

Fig. 4*A* compares the geminate recombination of NO to the three proteins in the presence of both arginine and BH_4. Under these conditions, all three samples formed the ferric high-spin unliganded heme after photo-dissociation (Figs. 1 and 2*A*). The kinetics of NO rebinding differ in the hundreds of picoseconds: $\tau_2 = 425 \pm 30$ ps for the wild type compared with $\tau_2 = 230 \pm 30$ ps for W457A/F. The constant term increases somewhat, from 13 to 24% by mutation of W to A or F, respectively (Fig. 2 and Table I).

Fig. 4*B* compares the rebinding of NO to the reduced proteins in the presence of arginine and BH_4. The kinetics of NO rebinding to either W457A/F are very similarly fitted by two exponential terms, $\tau_1 = 34 \pm 6$ ps and $\tau_2 = 350 \pm 70$ ps and a constant one. These decays are much faster than that obtained with the wild-type protein, especially in the tens of picoseconds. The weight of the first exponential term largely increases from 0.34 in iNOSoxy to 0.54 in both W457A and W457F. As shown in Table I, the recombination of NO to the ferrous heme does not depend on the NO concentration in the range 0.1–10%.

Molecular Dynamics Simulations

Simulations of the dynamics of NO dissociation were performed by using the structure of BH_4-bound iNOSoxy (Protein Data Bank ID code 1NSI) (26, 28). Fig. 5 shows the structure of the reduced heme in the presence of arginine and pterin represented in *red*. Superimposed is the structure simulated in the absence of the cofactor depicted in *blue*. The pterin site is left empty by the absence of BH_4. To the best of our knowledge, there is no experimental evidence showing that the arginine is able to replace the missing pterin, as it occurs in eNOS (30). The two simulated structures differ in the tilt of Trp-457 when the pterin site remains vacant and in some accommodation of the heme propionate chains.

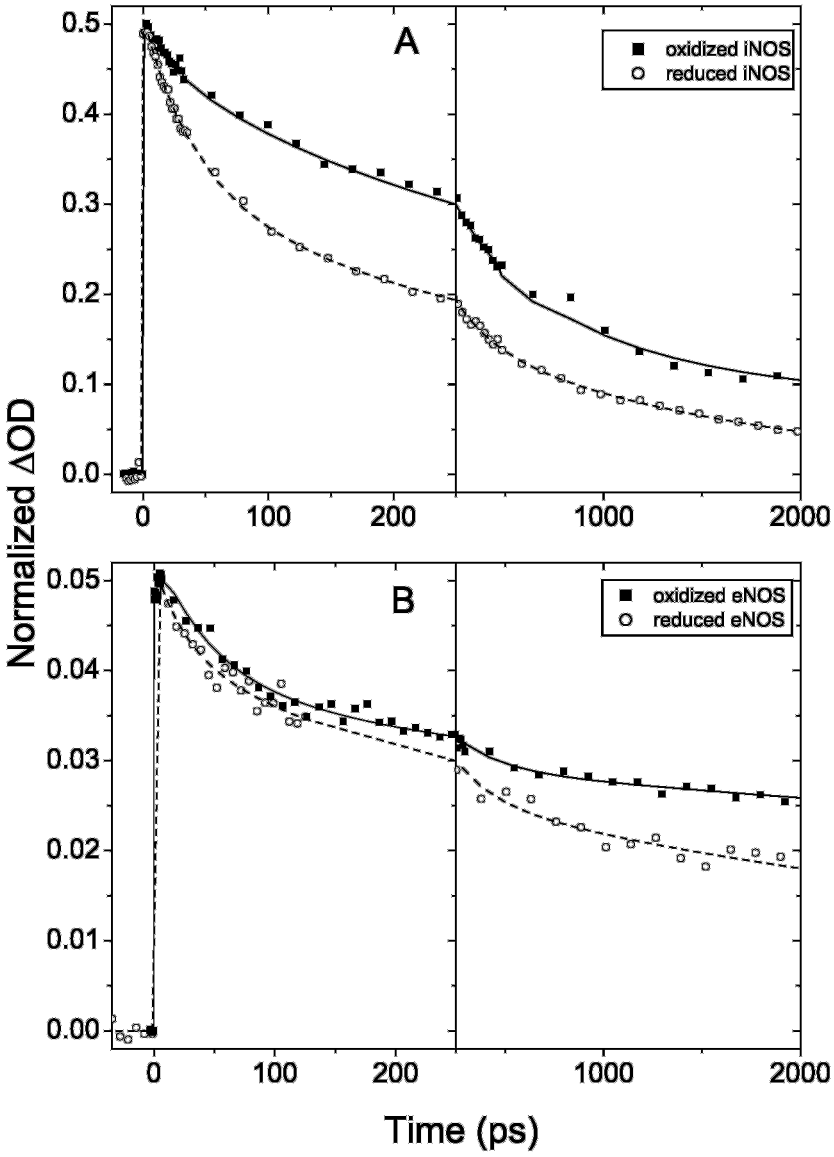

FIG. 3. **Comparison of the kinetics of geminate recombination of NO to the ferric and ferrous heme of iNOS and eNOS.** *A*, ■, iNOS ferric heme; and ○, ferrous heme. 67–80 μM protein in the presence of 20 mM arginine, 1 mM BH_4, 50 mM HEPES, pH 7.5, 5% glycerol, 3 mM DTT, 10% NO in the gas phase. *B*, ■, eNOS ferric heme; ○, ferrous heme (Refs. 31 and 32). 50 μM protein repleted with 0.5–0.6 BH_4 equivalent, 5 mM arginine, 50 mM HEPES, pH 7.5, 5% glycerol, 100 and 10% NO in the gas phase, respectively.

Fig. 5 also shows the position of NO, depicted in *green* (N atom) and *magenta* (oxygen atom) after a typical trajectory of 10 ps. The ligand remained confined in the heme pocket. The same dynamics were obtained independently of the presence of the pterin, suggesting that NO rebinding to the ferrous heme does not depend on the pterin, at least for 10–20 ps.

DISCUSSION

Effect of BH_4 on NO Rebinding to the Ferric Heme of iNOSoxy and W457A/F—Our transient absorption measurements probe the rebinding of NO to the heme once it is photodissociated; only intra-protein dynamics are relevant in the investigated time scales. The picosecond phase corresponds to NO rebinding that did not leave the heme pocket, whereas the nanosecond phase reflects the rebinding of NO molecules that left the heme pocket but were still in the protein. The former phase is probably lacking activation energy, whereas the latter process has to overcome an energy barrier. The upper limit of the probability of NO escape from the protein is given by the A_4 asymptotic value (Table I).

The geminate recombination rate is decreased in the picosecond range by the presence of BH_4, compared with BH_4-depleted proteins (Fig. 2*A*). This effect is enhanced in the mutated proteins. This clearly points to a rearrangement of the heme pocket induced by the pterin. No structure is available for BH_4-depleted iNOSoxy. Thus, we simulated the molecular dynamics based on the structure of BH_4-bound iNOSoxy to which the pterin was removed (Protein Data Bank ID code 1NSI; Ref. 26). The calculations, made on the ferrous nitrosyl, suggest a tilt of Trp-457 toward the vacant site of the missing pterin, compared with its position adopted in the presence of BH_4. The heme propionates adapt their position adequately to Trp-457 rotation (Fig. 5). This simulated change of Trp-457 position is likely to be relevant for the ferric heme, because it arises from steric rather than electronic coupling effects that may depend upon the valence of the heme iron (data not shown).

The larger effect of the pterin on the W457A than on WT probably reflects a larger rearrangement of the heme pocket arising from the smaller size of the Ala side chain compared with Trp. This effect may extend to remote residues, like those located at the protein solvent or the dimer interface. The smaller steric hindrance of Ala than Trp (with respect to that of BH_4) may explain the enhanced probability of NO escape in W457A than in iNOSoxy. W457F showed an intermediate effect (Fig. 2 and Table I). The slower rebinding of the NO molecules generated with excess energy is consistent with the

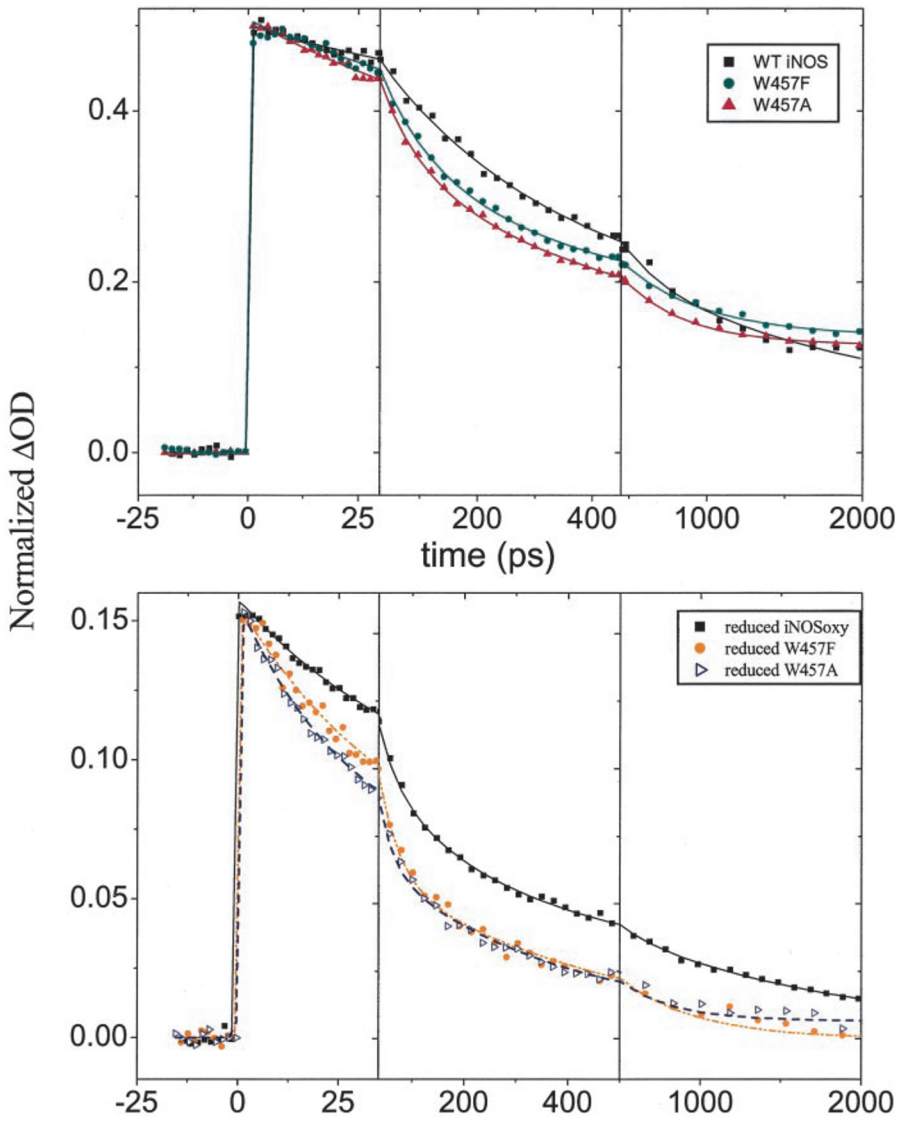

FIG. 4. **Effect of the mutation of Trp-457 on the geminate recombination of NO to the ferric heme (*A*) or ferrous heme (*B*) in the presence of 1 mM BH_4.** *A*, *black squares*, iNOSoxy; *blue circles*, W457F; *pink triangles*, W457A. *B*, *black squares*, iNOSoxy; *orange circles*, W457F; *blue triangles*, W457A. 67–80 μM protein, 50 mM HEPES, pH 7.5, 5% glycerol, in the presence of 20 mM arginine, 10% NO in the gas phase in *A* and 1% NO in the gas phase in *B*.

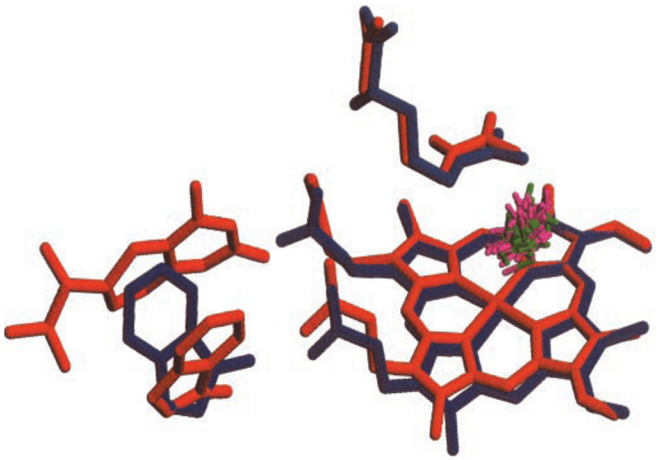

FIG. 5. **Typical trajectory of NO dissociation: structures of iNOS active site in the presence (*red*) or absence (*blue*) of the pterin 10 ps after the NO dissociation.** The positions at 100-fs interval of N (*green*) and O (*magenta*) atoms during a 10-ps trajectory are shown in stick representation.

increase in the energy barrier for recombination in the mutated proteins. This contrasts with the lack of such an effect in the WT protein

This control of NO release from NOS depends on the isoform and its specific redox state. The effect of BH_4 on the rate of NO rebinding to ferric iNOSoxy contrasts the lack of such dependence in the case of the ferric eNOS (31). It is opposite to the one observed on NO rebinding to the ferrous eNOS (32). The simulations show that NO (represented by *green* and *magenta bars*) remains localized on the heme over 10 ps independently of BH_4 (Fig. 5).

Such contrasting effects may arise from the topological changes in the BH_4-containing cavity of the two NOS isoforms (26, 33). Specifically, a residue of the H15 helix, eNOS Ala-446 is changed into iNOS Ile-462, the latter making a looser hydrogen bond with Asn-8 of BH_4 than the former. In addition, Met-120 in iNOS substitutes for Val-106, whose bulkier side chain makes a tighter contact with the pterin Asn-5 atom. The steric effect of this valine probably limits NO release in the presence of the cofactor.

Alternatively, the pterin could stabilize differently the iron-thiolate linkage of iNOS and of the endothelial enzyme, in turn affecting the heme redox potential (34). This hypothesis is consistent with the modification of the heme iron reactivity of iNOS by BH_4 (8). The pterin increases the coupling between the heme and the cofactor and, in turn, lowers the heme redox potential of iNOS from −347 to −295 mV without and with pterin, respectively (8). This effect probably results from the formation of the key hydrogen bonds between BH_4 and the heme propionate that increases the heme planarity. The redox

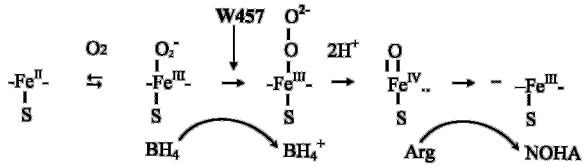

SCHEME 1. Scheme 1 is part of Fig. 1 from Wei *et al.* (10) showing the redox role of the BH_4 cofactor in donating an electron to ferrous-oxy complex, which is facilitated by Trp-457, located between the tetrahydrobiopterin and the heme propionate.

potential of the heme of eNOS and iNOS with BH_4 and bound arginine are similar: −250 to −260 mV (8, 35, 36), but the effect of the pterin on eNOS redox potential is unknown. Nevertheless, changes in heme geometries have been linked to variations in the redox potential of heme irons. For example, addition of arginine promotes changes of heme geometry, which are indicated by the observation of low-frequency, pyrole vibrational modes (35). It also induces a large decrease in the geminate recombination rate of the ferric enzyme (31). This assumed role of the pterin in modulating the strength of the Fe-S bond and, in turn, the redox potential in a specific manner for each of the two isoforms waits for further experimental support.

Effect of the Heme Redox State on the Geminate Recombination—Considering the general scheme of NOS catalysis proposed by Santolini *et al.* (21), the relative reaction rates of Fe(II)-NO and Fe(III)-NO govern the activity of each isoform (Scheme 1). Specifically, iNOS is characterized by the relatively rapid oxidation rate of its ferrous heme-NO complex compared with the heme reduction rate, implying that the ferrous heme-NO species does not accumulate appreciably during iNOS catalysis in the absence of NO build-up in solution (20–21). The ferric nitrosyl complex is the species that accumulates during catalysis and regulates NO release from iNOS. This fact is nicely reflected by the large differences in both rates and the extent of recombination of the two redox species (shown in Fig. 3). The NO recombination to the reduced heme after 2 ns reaches at least 92%, in contrast with the 80% rebinding to the ferric iron, in agreement with the large difference in their respective k_{off} values (21).

As for the geminate recombination of the endothelial isoform (Fig. 3*B*), the decays of both oxidized and reduced heme are very similar in the ps range, in contrast with the large difference observed in iNOSoxy on the same timescale. The ps-range decay probes the close environment of the heme, the structure of which does not differ much in both redox states of eNOS (34, 37). Despite the lack of the x-ray data of the reduced iNOSoxy, the large difference in NO recombination to iNOS ferric and ferrous states suggests some modifications of the structure of the enzyme and/or the coupling between the heme and the pterin according to its redox state.

The decays of oxidized and reduced eNOS differ in the ns timescale. Both decays were much slower in eNOS than in iNOS. This result is consistent with a more efficient NO release from eNOS than from iNOS once NO is formed. The lack of ferrous nitrosyl complex during eNOS catalysis points out that the efficiency of eNOS catalysis is controlled by the heme reduction. However, there is a discrepancy between our geminate rebinding data of ferrous nitrosyl eNOS and iNOS and the reported k_{off} value of $\sim 10^{-4}$ s^{-1} for both enzymes (21). The two types of data should vary accordingly if the probability of Fe(II)-NO bond thermal cleavage is comparable in iNOS and eNOS. However, there are no available data on the relative strength of this bond in the two NOS isoforms.

Effect of the Trp-457 Mutation—The effect of the W457A/F mutation on the geminate recombination to the ferric BH_4-repleted heme is mainly restricted to the hundreds of picoseconds time scale, which corresponds to NO rebinding from the heme pocket (Fig. 4*A*). This confinement is consistent with the conservation of the key hydrogen-bonding of the BH_4 site in the mutated proteins (16). The mutation also induces a somewhat larger asymptotic term in the mutated proteins, 0.25 and 0.23 ± 0.03 for W457A and W457F respectively, compared with 0.13 ± 0.02 in WT. However, the large decrease of NO yield induced by the mutation cannot be explained by the enhancement of geminate recombination rate. The decreased efficiency of the catalysis is thus the major effect of the mutation (17, 19).

The W457A/F mutation increases the rate of NO rebinding to the ferrous heme in the mutated proteins relative to that in the wild-type one (Fig. 4*B*). NO mainly remains restricted to the heme pocket of the mutated proteins, because most of the rebinding is accomplished within 500 ps. The ferrous heme-NO complex of iNOS undergoes oxidization and forms nitrate in the "futile" reaction cycle. Thus, the mutation should improve the efficiency of the futile cycle by its effect on the dynamics of NO rebinding to Fe(II), provided the rate of Fe(II)-NO oxidation by oxygen is unchanged by the mutation. However, NO rebinding to the ferrous heme is already quite efficient in the wild-type enzyme, so the overall effect of the mutation by improving the futile cycle may be minimal on the steady-state catalysis.

Acknowledgments—We gratefully acknowledge Dr. A.-L. Tsai and V. Berka for the gift of eNOS, and Drs. J. Santolini and C. S. Raman for stimulating discussions.

REFERENCES

1. Stuehr, D. J. (1999) *Biochim. Biophys. Acta* **1411,** 217–230
2. Alderton, W., Cooper, C. E., Knowles, R. G. (2001) *Biochem. J.* **357,** 593–615
3. Rusche, K. M., Spiering, M. M., and Marletta, M. A. (1998) *Biochemistry* **37,** 15503–15512
4. Abou-Soud, H. M., Wu, C., Ghosh, D. K., and Stuehr, D. J. (1998) *Biochemistry* **37,** 3777–3786
5. Rusche, K. M., and Marletta, M. A. (2001) *J. Biol. Chem.* **276,** 421–427
6. Chen, P. F., and Wu, K. K. (2000) *J. Biol. Chem.* **275,** 13155–13163
7. Mayer, B., Wu, C., Gorren, A. C. F., Pfeiffer, S., Schmidt, K., Clark, P., Stuehr, D. J., and Werner, E. R. (1997) *Biochemistry* **36,** 8422–8427
8. Presta, A., Weber-Main, A. M., Stankovitch, M. T., and Stuehr, D. J. (1998) *J. Am. Chem. Soc.* **120,** 9460–9465
9. Bec, N., Gorren, A. C., Voelker, C., Mayer, B., and Lange, R. (1998) *J. Biol. Chem.* **273,** 13502–13508
10. Wei, C. C., Wang, Z., Wang, Q., Meade, A. L., Hemann, C., Hille, R., and Stuehr, D. J. (2001) *J. Biol. Chem.* **276,** 315–319
11. Stuehr, D. J., Pou, S., and Rosen, G. M. (2001) *J. Biol. Chem.* **276,** 14533–14536
12. Hurshman, A. R., and Marletta, M. A. (1995) *Biochemistry* **34,** 5627–5634
13. Crane, B. R., Arvai, A. S., Gachhui, R., Wu, C., Ghosh, D. K., Getzoff, E., Stuehr, D. J., and Tainer, J. A. (1997) *Science* **278,** 425–431
14. Crane, B. R., Arvai, A. S., Ghosh, D. K., Wu, C., Getzoff, E., Stuehr, D. J., and Tainer, J. A. (1998) *Science* **279,** 425–431
15. Crane, B. R., Arvai, A. S., Ghosh, D. K., Getzoff, E., Stuehr, D. J., and Tainer, J. A. (2000) *Biochemistry* **39,** 4608–4621
16. Aoyagi, M., Arvai, A. S., Ghosh, D. K., Stuehr, D. J., Tainer, J. A., and Getzoff, E. (2001) *Biochemistry* **40,** 12826–12832
17. Ghosh, D. K., Wolan, D., Adak, S., Crane, B. R., Kwon, N. S., Tainer, J. A., Getzoff, E., and Stuehr, D. J. (1999) *J. Biol. Chem.* **274,** 24100–24112
18. Wang, Z. Q., Wei, C. C., Ghosh, S., Meade, A. L., Hemann, C., Hille, R., and Stuehr, D. J. (2001) *Biochemistry* **40,** 12819–12825
19. Wang, Z. Q., Wei, C. C., and Stuehr, D. J. (2002) *J. Biol. Chem.* **277,** 12830–12837
20. Abou-Soud, H. M, Ichimori, K., Nakazawa, H., and Stuehr, D. J. (2001) *Biochemistry* **40,** 6876–6881
21. Santolini, J., Meade, A. L., and Stuehr, D. J. (2001) *J. Biol. Chem.* **276,** 48887–48898
22. Eberlein, G., Bruice, T. C., Lazarus, R. A., Henrie, R., and Benkovic, S. J. (1984) *J. Am. Chem. Soc.* **106,** 7916–7924
23. Martin, J. L., and Vos, M. H. (1992) *Annu. Rev. Biophys. Biomol. Struct.* **21,** 199–222
24. Petrich., J., Poyart, C., and Martin, J.-L. (1988) *Biochemistry* **27,** 4049–4060
25. Press, W. H., Teukolsky, S. A., Vetterling, W. T., Flannery, B. P. (1988) *Numerical Recipes*, Cambridge University Press, Cambridge, UK
26. Li, H., Raman, C. S., Glaser, B. E., Young, T. A., Parkinson, J. F., Whitlow, M., and Poulos, T. L. (1999) *J. Biol. Chem.* **274,** 21276–21284
27. Lambry, J.-C., Vos, M. H., and Martin, J.-L. (1999) *J. Phys. Chem. A* **103,** 10132–10137
28. Berman, H. M., Westbrook, J., Feng, Z., Gilland, G., Bhat, T. N., Weissig, H., Shindyalov, I. N., and Bourne, P. E. (2000) *Nucleic Acids Res.* **28,** 235–242

29. Hurshman, A. R., and Marletta, M. A. (2002) *Biochemistry* **41,** 3439–3456
30. Raman, C. S., Li, H., Martasek, P., Kral, V., Masters, B. S. S., and Poulos, T. (1998) *Cell* **95,** 939–950
31. Négrerie, M., Berka, V., Vos, M. H., Liebl, U., Lambry, J. C., Tsai, A. L., and Martin, J. L. (1999) *J. Biol. Chem.* **274,** 24694–24702
32. Slama-Schwok, A., Négrerie, M., Berka, V., Lambry, J. C., Tsai, A. L., Vos, M. H., and Martin, J. L. (2002) *J. Biol. Chem.* **277,** 7581–7586
33. Fishmann, T. O., Hruza, A., Niu, X. D., Fossetta, J. D., Lunn, C. A., Dolphin, E., Prongay, A. J., Reichert, P., Lundell, D. J., Narula, S. K., and Weber, P. C. (1999) *Nat. Struct. Biol.* **6,** 233–242
34. Raman, C. S., Martasek, P., and Masters, B. S. S. (2000) *The Porphyrin Handbook* (Kadish, K. M., Smith, K. M., and Guilard, R., eds) Vol. 4, Academic Press, London
35. Schelvis, J. P., Berka, V., Babcock, G. T., and Tsai, A. L. (2002) *Biochemistry* **41,** 5695–5701
36. Du, M., Ye, V., Berka, V., Wang, L. H., and Tsai, A. L. (2003) *J. Biol. Chem.* **278,** 6002–6011
37. Kotsonis, P., Frohlich, L. G., Raman, C. S., Li, H., Berg, M., Gerwig, R., Groehn, V., Kang, Y., Al-Masoudi, N., Taghavi-Moghadam, S., Mohr, D., Munch, U., Schnabel, J., Martasek, P., Masters, B. S., Strobel, H., Poulos, T., Matter, H., Pfleiderer, W., and Schmidt, H. H. (2001) *J. Biol. Chem.* **276,** 49133–49141